

Sleep-Based Homeostatic Regularization for Stabilizing Spike-Timing-Dependent Plasticity in Recurrent Spiking Neural Networks

Andreas Massey Aliaksandr Hubin Stefano Nicheli Solve Sæbø

January 14, 2026

Abstract

Spike-timing-dependent plasticity (STDP) provides a biologically-plausible learning mechanism for spiking neural networks (SNNs); however, Hebbian weight updates in architectures with recurrent connections suffer from pathological weight dynamics: unbounded growth, catastrophic forgetting, and loss of representational diversity. We propose a neuromorphic regularization scheme inspired by the synaptic homeostasis hypothesis: periodic offline phases during which external inputs are suppressed, synaptic weights undergo stochastic decay toward a homeostatic baseline, and spontaneous activity enables memory consolidation. We demonstrate that this sleep-wake cycle prevents weight saturation while preserving learned structure. Empirically, we find that low to intermediate sleep durations (10–20% of training) improve stability on MNIST-like benchmarks in our STDP-SNN model, without any data-specific hyperparameter tuning. In contrast, the same sleep intervention yields no measurable benefit for the surrogate-gradient spiking neural network (SG-SNN). Taken together, these results suggest that periodic, sleep-based renormalization may represent a fundamental mechanism for stabilizing local Hebbian learning in neuromorphic systems, while also indicating that special care is required when integrating such protocols with existing gradient-based optimization methods.

Keywords: spiking neural networks, STDP, homeostasis, online learning, neuromorphic computing

1 Introduction

Spiking neural networks (SNNs) encode information through the spatiotemporal distribution of discrete spike events, enabling efficient event-driven computation on neuromorphic devices [Su et al., 2023]. This temporal sparsity yields orders-of-magnitude reductions in power consumption compared to dense, continuous-valued architectures [Isik et al., 2024]. However, the learning landscape for SNNs remains both inefficient and poorly understood [Akil et al., 2021], particularly concerning the stability and convergence of biologically plausible local learning rules [Stratton et al., 2022].

Spike-timing-dependent plasticity (STDP) emerges naturally as the canonical local learning rule for SNNs [Song et al., 2000]. Weight modifications depend solely on the millisecond-scale timing differences between pre- and postsynaptic spikes: when presynaptic activity temporally precedes postsynaptic firing, weights strengthen; when the order reverses, weights weaken. This causality-respecting update rule is not only biologically faithful, but also theoretically motivated as it implements credit assignment through temporal adjacency and emerges from principles of spike coincidence detection [Jayabal et al., 2024, Chauhan et al., 2018]. Yet, in recurrent architectures essential for temporal processing and internal state maintenance, STDP exhibits severe pathologies. Recurrent connectivity amplifies initial weight perturbations through positive-feedback loops, driving three intertwined failure modes: (i) **weight saturation**, where unrestricted Hebbian potentiation of co-active synapses drives weights toward unbounded values or clipping limits [Gilson et al., 2010]. The former creates catastrophic instabilities, while the latter eliminates further learning capacity; (ii) **representational collapse**, where weight-coupling induces spurious correlations that erode discriminative structure [Akil et al., 2021]; and (iii) **catastrophic forgetting**, where sequential task learning overwrites previously-learned representations [Tadros et al., 2022].

The field has pursued two main approaches to stabilize STDP, each with significant costs. First, *homeostatic mechanisms* employ global normalization schemes: synaptic scaling re-normalizes weight distributions toward firing-rate targets, intrinsic plasticity adapts neuronal thresholds, and structural plasticity modifies connectivity [Carlson et al., 2013]. While effective, these approaches sacrifice strict locality - requiring global firing-rate statistics - and raise concerns about biological implausibility - synaptic scaling is typically modeled as multiplicative global factors rather than local mechanisms [Qiao et al., 2016]. Second, *surrogate-gradient* (SG) methods circumvent spike non-differentiability by replacing discontinuities with smooth membrane proxies during backpropagation, enabling error-based weight updates [Huh and Sejnowski, 2017]. SG methods can thus be coupled with standard ℓ_1 or ℓ_2 regularization and achieve solid accuracy for SNNs (>97% on MNIST), but incur substantial costs that contradict the motivation for SNNs: they require error backpropagation (sacrificing locality), demand significant memory for gradient storage, utilize loss functions, and eliminate the event-driven sparsity that is arguably one of the strongest benefits of neuromorphic computation [Li et al., 2024, Wang et al., 2023].

We propose a third approach grounded in the synaptic homeostasis hypothesis (SHy), a neuroscientific theory positing that sleep performs activity-weighted synaptic renormalization to maintain stability and consolidate learning [Tononi and Cirelli, 2014]. During biological sleep, high-activity synapses undergo more aggressive down-scaling than low-activity synapses, achieving both weight renormalization and selective pruning of task-irrelevant connections, as explored in prior sleep-inspired neuromorphic models like Tadros et al. [2022], Kinoshita et al. [2025], Nere et al. [2013]. We transpose this principle into a neuromorphic algorithm: periodic sleep/wake cycles similar to Thiele et al. [2017]: During the sleep phase, (1) external inputs are suppressed, (2) synaptic weights undergo controlled power-law decay toward a homeostatic baseline, and (3) spontaneous neural activity, driven solely by intrinsic membrane noise inspired by Ma et al. [2023] and Deperrois et al. [2022], permits continued STDP application, enabling consolidation through implicit replay. The latter has demonstrated improved intra-class consistency and reduced risks of overfitting to data [Deperrois et al., 2022, Hoel, 2021, Tadros et al., 2022]. Critically, this mechanism preserves full locality (requiring only pre- and

post-synaptic statistics), adds negligible computational overhead, and remains compatible with neuromorphic hardware. Moreover, we highlight a key distinction in how sleep-based homeostasis interacts with different learning paradigms. Sleep phases are mechanistically compatible with Hebbian learning, as both operate on local activity statistics. In contrast, few hybrid STDP/backpropagation (BP) approaches have been evaluated in SNNs, and existing methods typically attempt to circumvent locality constraints by introducing global reward signals or probabilistic learning rules. This reflects a fundamental incompatibility: STDP, by construction, cannot directly support BP’s reliance on global error gradients. Our experimental results are consistent with this view. While spontaneous activity and noisy weight reductions during sleep may, in principle, aid surrogate-gradient-trained SNNs in escaping poor local optima, we find no evidence that this translates into systematic improvements in learning performance¹.

Our contributions are threefold. First, we present a principled sleep-wake mechanism combining homeostatic weight decay with spontaneous replay, deriving stability conditions showing that periodic renormalization bounds weight growth and maintains representational structure, consistent with [Capone et al., 2019]. Second, we suggest drivers to prevent performance-saturation: consolidation-through-replay, and maintained homeostatic balance—with mechanistic explanations. Third, we provide empirical validation on MNIST-family benchmarks, showing that intermediate sleep durations (10%–20% of baseline training) reliably improve performance in our STDP-based model, whereas no sleep regime yields gains for the surrogate-gradient SNN model.

The remainder of the paper is organized as follows: Section 2 describes the methods used in this work, including the two spiking neural network implementations under study, their architectures, learning rules, and sleep-wake regularization protocols. As an initial validation step, we first evaluate the STDP-SNN on a controlled toy classification task to verify stable learning dynamics under unsupervised STDP, before scaling to MNIST-family benchmarks with both models. Section 3 presents the results. Section 4 discusses the broader implications for neuromorphic hardware and future research directions.

2 Methods

2.1 Overview

We compare two spiking neural network implementations that differ in architecture and learning paradigm, but are both augmented with the same sleep-inspired homeostatic regularization mechanism. The first model, the spike-timing-dependent plasticity spiking neural network (STDP-SNN), is a recurrent excitatory–inhibitory architecture trained using local STDP and iSTDP learning rules. It is implemented from scratch in `numpy` with `numba` acceleration and explicitly models leaky integrate-and-fire neuron dynamics, synaptic plasticity, and sleep–wake cycles. During sleep phases, synaptic weights undergo noise-driven renormalization while STDP remains active, enabling replay-like consolidation.

¹There have been some attempts to combine surrogate-methods with STDP, for example, the noisy-SNN (NSNN) model developed by Ma et al. [2023]. They leverage noisy membrane activity to ensure a more robust network and feed the loss into the membrane potential, similar to other surrogate-methods.

The second model, the surrogate-gradient spiking neural network (SG-SNN), is implemented using the `snntorch` framework and consists of feedforward linear layers coupled with leaky integrate-and-fire units, trained via surrogate-gradient backpropagation. In this setting, sleep is introduced by periodically interrupting task-driven training to apply the same weight-decay and noise mechanisms, but without ongoing STDP.

Consequently, sleep plays a distinct functional role in the two models: facilitating replay-based consolidation in the STDP-SNN, while acting solely as a stochastic regularizer in the surrogate-gradient regime.

All code for the STDP-SNN model is publicly available at [Massey \[2025\]](#).

2.2 STDP-model

The STDP-SNN serves as our primary biologically inspired model, combining local spike-timing-dependent plasticity with a periodic, sleep-inspired homeostatic regularization mechanism. The network is trained in an unsupervised manner using exclusively local learning rules, while stability is enforced through noisy weight renormalization during interleaved sleep phases. This design allows the model to learn class-structured representations while avoiding the pathological weight dynamics typically associated with recurrent STDP-based networks.

2.2.1 Architecture

To construct our network, we drew inspiration from prior work on unsupervised clustering in spiking neural networks [Zenke et al., 2015], which demonstrated that recurrent excitatory-inhibitory architectures trained with STDP can self-organize class-selective representations. This class of models is particularly well suited for studying stability in Hebbian learning, as recurrent excitation amplifies small weight perturbations and is therefore prone to pathological dynamics in the absence of explicit regularization. By adopting a similar architecture, we intentionally place our model in a challenging regime where uncontrolled STDP is known to fail, allowing us to directly assess whether sleep-inspired homeostatic mechanisms can stabilize learning without sacrificing locality.

To keep the results comparable, we chose the following network parameters: a Poisson process input encoding into spikes layer ($N_{\text{in}} = 225$ neurons), a recurrent excitatory readout layer ($N_{\text{exc}} = 200$), and a lateral inhibitory layer ($N_{\text{inh}} = 50$). Note that Zenke et al. [2015] also included a recurrent weight within the lateral inhibitory layer. We opted out of this due to increased complexity in estimating hyper-parameters. Connectivity is random and sparse: $P_{\text{in} \rightarrow \text{exc}} = 10\%$, $P_{\text{exc} \rightarrow \text{exc}} = 15\%$, $P_{\text{exc} \rightarrow \text{inh}} = 20\%$, $P_{\text{inh} \rightarrow \text{exc}} = 25\%$, with no self-connections. This architecture captures key sensory cortex properties: feedforward thalamic input, recurrent excitatory dynamics, and local inhibitory control.

2.2.2 Neuron model

Each neuron integrates synaptic inputs via leaky integrate-and-fire (LIF) dynamics:

$$\tau_m \frac{dU_i(t)}{dt} = -(U_i(t) - U_{\text{rest}}) + R_m I_i^{\text{syn}}(t) + \xi_i(t), \quad (1)$$

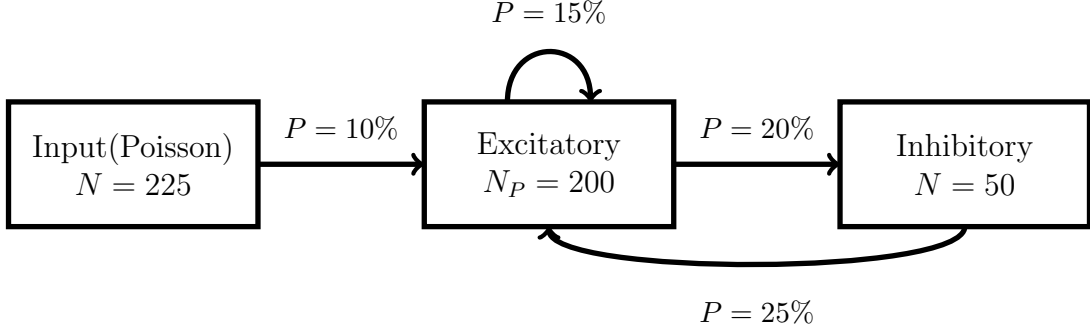


Figure 1: Network architecture: three-layer SNN with feedforward input ($P = 10\%$), recurrent excitation ($P = 15\%$), and lateral inhibition ($P = 25\%$). Sparse connectivity enables event-driven computation.

where $U_i(t)$ is the membrane potential, τ_m is the time constant, R_m is the membrane resistance, U_{rest} is the resting potential, $I_i^{\text{syn}}(t) = \sum_j w_{ij} S_j(t)$ is the synaptic current, and $\xi_i(t) \sim \mathcal{N}(0, \sigma^2)$ is intrinsic noise. When $U_i(t) \geq U_{\text{th}}^i(t)$, neuron i emits a spike ($S_i(t) = 1$) and resets to U_{rest} . The spike threshold is adaptive (preventing runaway firing):

$$\begin{aligned} \frac{dU_{\text{th}}^i(t)}{dt} &= U_{\text{th}}(0) + \alpha_i, \\ \frac{d\alpha_i}{dt} &= -\frac{\alpha_i}{\tau_{\text{th}}} + S_i(t)\delta, \end{aligned}$$

with baseline spike threshold $U_{\text{th}}(0)$, time constant τ_{th} , and jump amplitude δ . For example, with $\delta = 3$ we reduce the probability of prolonged spike trains, i.e., each time neuron i spikes, the spiking threshold increases by 3 mV ($\sim 6.5\%$ increase per postsynaptic spike).

2.2.3 Learning rule

Excitatory synapses update via spike-timing-dependent plasticity (STDP):

$$\Delta w_{ij}^{\text{exc}}(\Delta t) = \eta_{\text{exc}} \begin{cases} A_+ \exp(-\Delta t/\tau_+) & \text{if } \Delta t \geq 0 \\ -A_- \exp(\Delta t/\tau_-) & \text{otherwise,} \end{cases} \quad (2)$$

where $\Delta t = t_{\text{post}} - t_{\text{pre}}$ is spike timing, η_{exc} is the learning rate, and A_{\pm} , τ_{\pm} are learning amplitudes and time constants. Inhibitory synapses employ inverted STDP (iSTDP):

$$\Delta w_{ij}^{\text{inh}}(\Delta t) = \eta_{\text{inh}} \begin{cases} -A_+ \exp(-\Delta t/\tau_+) & \text{if } \Delta t \geq 0 \\ A_- \exp(\Delta t/\tau_-) & \text{otherwise,} \end{cases} \quad (3)$$

with η_{inh} being the (un-)learning rate. iSTDP ensures inhibitory neurons specialize for highly-active excitatory neurons, providing homeostatic load-balancing.

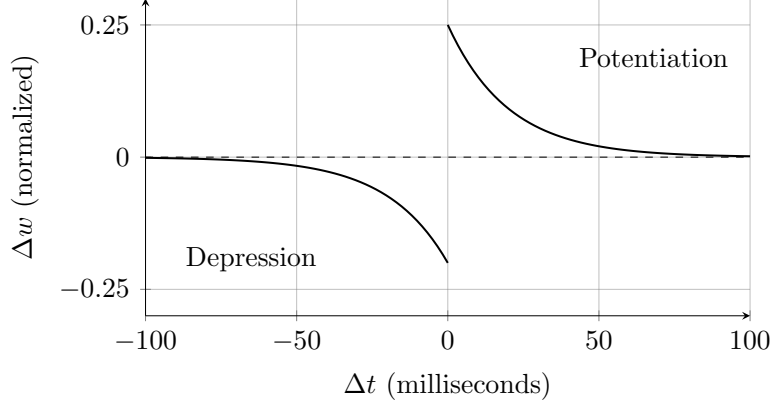


Figure 2: STDP learning window: weights strengthen (positive Δt) when presynaptic spike precedes postsynaptic, weaken (negative Δt) otherwise.

2.2.4 Sleep-protocol

The core innovation of this article is that we implemented a periodic sleep–wake schedule, controlled by the *sleep-ratio*. Time is partitioned into intervals of set lengths, *sleep interval*. At the start of each interval, the simulator enters a *hard-pause* sleep phase and performs up to

$$T_{\text{sleep}} = \max(1, \lfloor \text{sleep-ratio} \cdot \text{sleep interval} \rfloor)$$

virtual sleep iterations without advancing the real simulation time.

During sleep, weights decay via power-law dynamics that preserve relative ordering:

$$w_i(t+1) = w_{\text{tgt}} \left(\frac{w_i(t)}{w_{\text{tgt}}} \right)^\lambda, \quad (4)$$

where w_{tgt} is the target to which the function is converging and λ denotes the decay rate. During sleep, sensory input is suppressed (all stimulus spikes are set to zero), and membrane dynamics are driven by intrinsic noise, producing spontaneous spiking activity that can continue to elicit STDP updates. In addition, synaptic weights are renormalized toward target magnitudes via the sleep operator.

Sleep terminates when the sum of weights $\mathcal{W}_x(t)$ reaches w_x^{\min}

$$\mathcal{W}_x(t) \leq w_x^{\min} = \alpha_{\text{base}} \cdot \mathcal{W}_x(0), \quad \alpha_{\text{base}} < \alpha_{\text{trig}} \quad (5)$$

or when the *sleep interval* is surpassed without reaching w_x^{\min} .

2.2.5 Evaluation

To compute the accuracy, we first aggregated the average spike rates for each training sample, and standardized the feature vector into $\mu = 0$ and unit variance. Then, we perform dimensionality reduction on the standardized feature vector while maintaining 95% variance with PCA. Finally, we train a multinomial logistic regression (MLR) on the transformed features. The trained classifiers can then predict classes on the unseen test-data processed by the network.

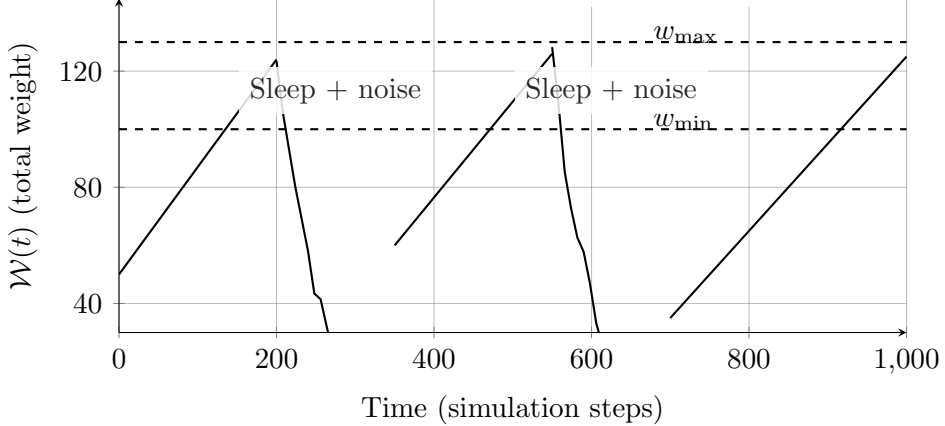


Figure 3: Weight dynamics: wake phases show deterministic linear STDP-driven growth; sleep phases show power-law regularization, Eq. 4 with superimposed random noise resembling realizations of Gaussian random variables, representing spontaneous neural activity during consolidation. System cycles robustly between wake (input-driven) and sleep (homeostatic noisy decay), maintaining weights within plausible intervals.

2.3 Toy geometric experiment

To assess the clustering behavior of the unsupervised STDP-SNN and to isolate the effects of sleep-based regularization from dataset-specific confounds, we designed a controlled toy classification task. This experiment serves as a diagnostic validation, allowing us to verify that the network develops stable and discriminative internal representations under local Hebbian learning before evaluating performance on large-scale image benchmarks.

2.3.1 Data

We used a synthetic geometric dataset consisting of 7,100 grayscale images at 15×15 resolution (Fig. 4a). Each image belongs to one of four geometric classes and is corrupted by additive Gaussian noise $\zeta_i \sim \mathcal{N}(0, 0.02)$ to introduce controlled variability while preserving class identity. Each stimulus was presented to the network for 100 ms.

The dataset was split into 6,000/100/1,000 samples for training, validation, and testing, respectively. Mini-batches were constructed to contain balanced class representations, ensuring that learning dynamics reflect clustering behavior rather than class-frequency effects.

2.3.2 Design

To estimate the efficacy of sleep, we compare model performance under two training regimes: sleep and no sleep. During the sleep condition, synaptic weights undergo periodic regularization, whereas in the no-sleep condition training proceeds continuously without these phases. In both regimes, synaptic weights are constrained to remain within their respective functional groups—excitatory or inhibitory—through sign-clamping, a mechanism that enforces fixed polarity by preventing weights from crossing the zero boundary and thereby changing their postsynaptic effect.

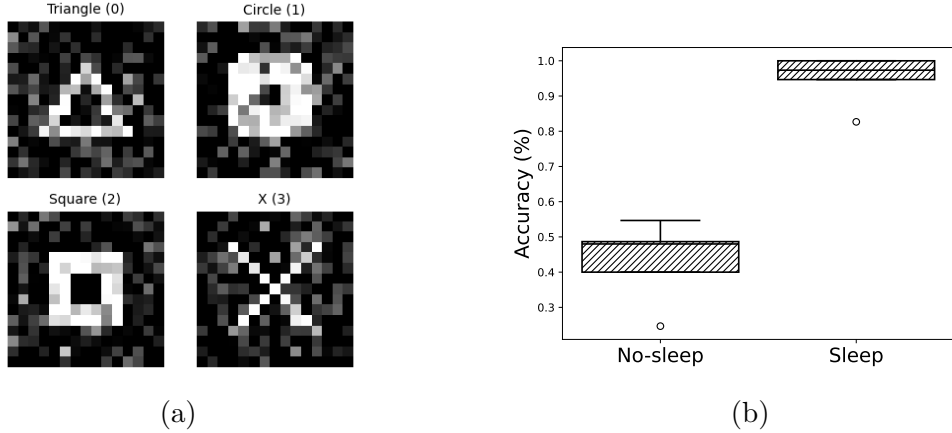


Figure 4: (a) training set composed of four geometric classes (triangle, circle, square, and cross), each subjected to Gaussian noise $\mathcal{N}(0, 0.02)$. All training examples use the same base shapes, with noise as the stochastic component introducing sample-by-sample variance. (b) shows accuracy attained with the *no-sleep* and *sleep* protocol.

2.3.3 Results

We observed that our sleep protocol combined with sign-clamping successfully stabilized the synaptic weights, whereas sign-clamping alone did not (see Figure 5). The sleep protocol achieved high accuracy (mean= 94.93, min= 82.67 and max= 100.00) within the span of 15 batches, while the *no-sleep* configuration achieved notably worse performance: (mean = 43.20, min = 24.67, and max = 54.67). In Fig. 5a, the weight averages and their min/max spans remain consistent across inhibitory and excitatory groups over training, whilst this is not the case for the *no-sleep* condition (see Fig. 5b). Within batches, this trend is also evident: Fig. 5c shows the within-batches dynamics: with the sleep protocol active, weights stay within bounded ranges yet still exhibit healthy heterogeneity. Meanwhile, Fig. 5d demonstrates how weights quickly explode without proper regularization methods in place.

In contrast, removing the sleep phase leads to rapid instability. Even within a single batch, weights begin to diverge; note the difference in y-axis scales between the sleep and no-sleep conditions, ultimately disrupting learning. This degradation is reflected in Fig. 6, where the *no-sleep* model 6b, shows impaired clustering structure. Because the sleep protocol restrains weight growth while preserving variability, it yields more stable performance and provides a clear class separation in this example.

2.4 Surrogate-gradient model

While the preceding sections focus on stabilizing fully local STDP in a recurrent E/I SNN, it remains unclear whether the observed gains are specific to Hebbian learning or reflect a more general regularization effect. To disentangle these factors, we introduce a second model trained with global error-driven optimization. This surrogate-gradient model provides a strong point of reference for (i) predictive performance under BPTT and (ii) whether the same sleep intervention transfers to gradient-based SNN training.

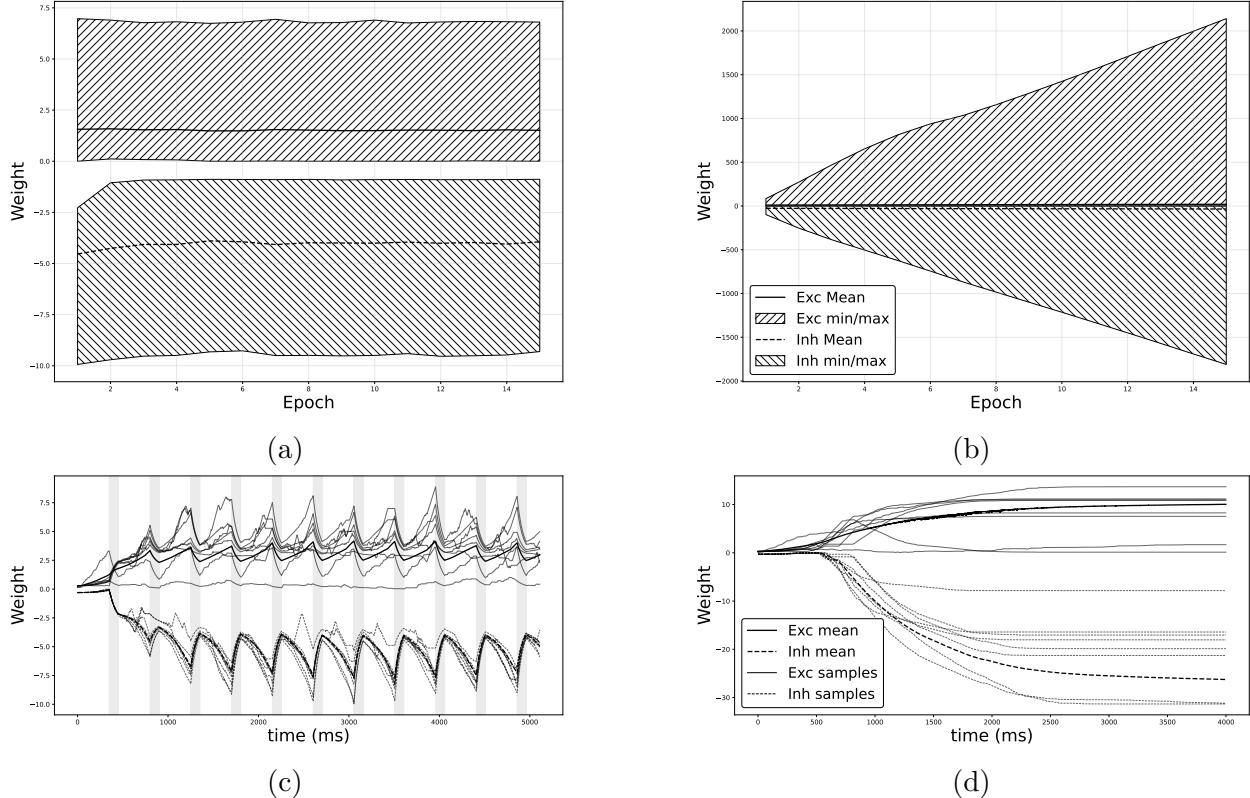


Figure 5: (a) denotes average excitatory and inhibitory weights across batches training with sleep regularization. The grey area capture min and max weights per batch. (b) denotes the same, but without sleep to stabilize learning. (c) shows weight changes across a single batch training session with the sleep protocol active. Along the x-axis, we plot time in milliseconds, and along the y-axis, we plot change in weights. Similar to (d), stippled lines represent inhibitory weights and solid lines excitatory min/max and mean weights.

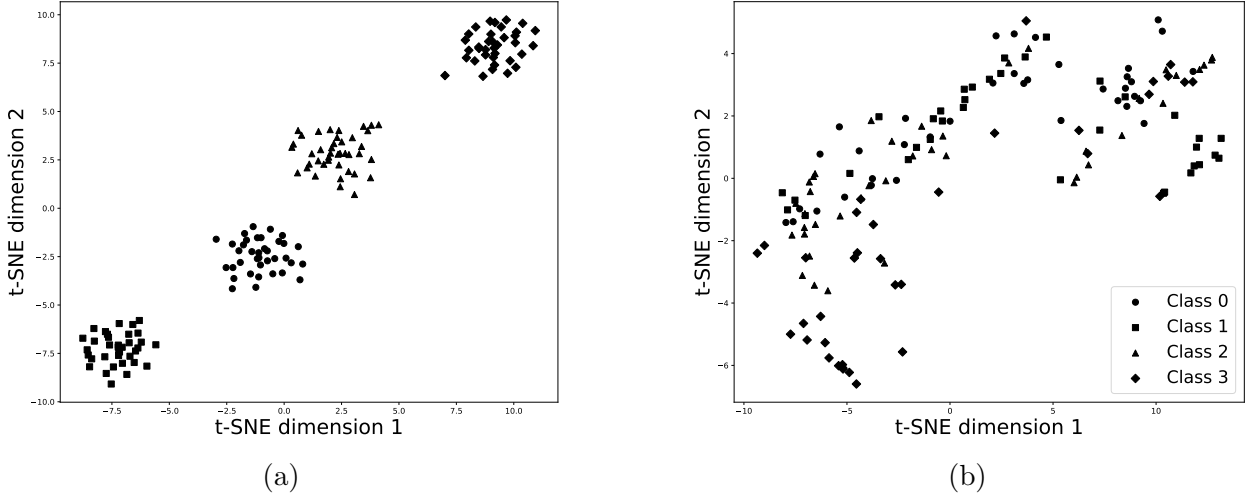


Figure 6: Comparison plot of t -SNE across sleep (a) and no-sleep (b) training paradigms. Both plots show t -SNE visualization of spike-rate vectors binned by training sample. Each geometric shape corresponds to a distinct class, and each point represents a test observation embedded into the t -SNE-reduced space.

2.4.1 Architecture

The network is a two-layer multilayer perceptron (MLP) with spiking dynamics:

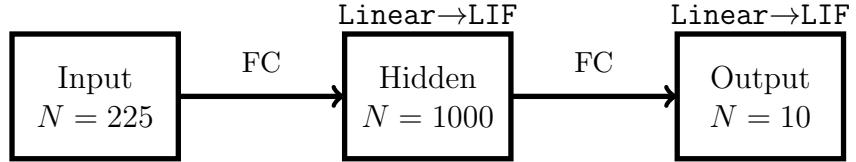


Figure 7: Surrogate-gradient baseline: feedforward spiking MLP (225–1000–10) implemented as fully-connected synapses followed by LIF dynamics (`nn.Linear→snn.Leaky`).

implemented as two fully-connected layers (`Linear`) followed by leaky integrate-and-fire (LIF) neurons (`snn.Leaky`). The architecture is purely feedforward (i.e. no recurrent connections as in the STDP-model). Each static input image is presented for $T = 100$ discrete simulation steps; the temporal dimension arises from the LIF state dynamics rather than time-varying spike-based input.

2.4.2 Neuron model

Each spiking layer uses a discrete-time LIF neuron with membrane decay parameter $\beta = 0.95$. Let $U(t)$ denote the membrane potential and $S(t) \in \{0, 1\}$ the emitted spike at time step t . In each layer, the membrane is updated according to the standard LIF recurrence (cf. Eq. 1), and a spike is generated by threshold crossing:

$$S(t) = H(U(t) - U_{\text{thr}}),$$

where $H(\cdot)$ is the Heaviside step function.

2.4.3 Learning rule

For comparison, we also implement surrogate-gradient (SG) training, in which the non-differentiable spike function is replaced by a smooth proxy during backpropagation. Forward pass: neurons generate spikes via the deterministic LIF threshold crossing rule (Equation 1 with a shifted Heaviside step function):

$$S_i(t) = \begin{cases} 1 & \text{if } U_i(t) \geq U_{thr} \\ 0 & \text{if } U_i(t) < U_{thr}. \end{cases} \quad (6)$$

During backpropagation, the spike nonlinearity is replaced by an arctangent-shaped surrogate $\tilde{S}_i(t)$, providing a smooth approximation to the threshold function and enabling gradient flow.

$$\tilde{S}_i(t) = \frac{1}{\pi} \arctan \left(\pi U_i(t) \frac{\alpha}{2} \right) \quad (7)$$

based on Fang et al. [2021], where α is the constant factor which determines the shape of the surrogate gradient. Weights are then updated via standard gradient descent on the task loss (\mathcal{L}):

$$w_{ij}(t+1) \leftarrow w_{ij}(t) - \alpha_{SG} \frac{\partial \mathcal{L}}{\partial w_{ij}(t)}, \quad (8)$$

where α_{SG} is the learning rate for SG training.

2.4.4 Sleep protocol

To investigate whether sleep-based regularization can also benefit SG-trained SNNs, we apply the same sleep-wake protocol described above. During wake phases, the network processes task-driven input, and STDP is disabled (gradients govern all updates). During sleep phases, we suppress external input ($I^{\text{task}} = 0$), maintain intrinsic noise in the membrane potential, and apply the same stochastic weight decay as in (4).

Unlike Hebbian training, where STDP continues during sleep and enables replay-based consolidation, in SG training, the sleep mechanism provides stochastic perturbations that may help escape suboptimal local minima in the error landscape. However, the multiplicative decay also disrupts the gradient-based weight updates. The net effect, thus, is expected to depend critically on sleep magnitude: at low sleep rates, noise-driven exploration may provide modest benefits by allowing to escape local extrema of the loss; at high rates, decay will likely dominate and degrade completely SG convergence.

2.4.5 Evaluation

Training minimizes a time-accumulated classification objective. For each input sample, the network produces an output spike vector $\mathbf{s}^{(2)}(t) \in \{0, 1\}^C$ at each simulation step $t \in \{1, \dots, T\}$, where $C = 10$ classes. We compute cross-entropy at every step and sum over the stimulus window:

$$\mathcal{L} = \sum_{t=1}^T \text{CE}(\mathbf{s}^{(2)}(t), y), \quad (9)$$

and update the synaptic parameters of the linear layers using Adam.

To obtain a single class prediction from the spiking output, we apply spike-count decoding at the final layer. Let $\mathbf{c} = \sum_{t=1}^T \mathbf{s}^{(2)}(t)$ denote class-wise spike counts; the predicted label is

$$\hat{y} = \arg \max_{k \in \{1, \dots, C\}} c_k. \quad (10)$$

Accuracy is reported as the fraction of samples with $\hat{y} = y$ on the validation and test sets.

2.5 MNIST-family experiment

To formally evaluate our models, we trained them on the MNIST-family of datasets: KMNIST, MNIST, FMNIST and NotMNIST.

2.5.1 Data

Each dataset contains 60,000 images for training and 10,000 for testing. Due to computational constraints with our STDP-SNN model, each image is 15×15 and each run consisted of a single epoch-run with 6,000 randomly drawn images until an even class distribution was achieved for both models. Each batch was subsequently validated with 100 samples and, finally, tested on 1,000 test samples similar to the toy experiment. To compare the effect of sleep, we trained our model on 11 varying sleep rates (0% to 100%, with 10% increments). In addition, to improve statistical confidence while ensuring comparability across sleep rates, we trained the model five times per sleep rate using a fixed set of five random seeds, reused across all sleep conditions. The total number of runs can be expressed as

$$\text{total runs} = \text{seeds} \times \text{sleep rates} \times \text{datasets} \quad (11)$$

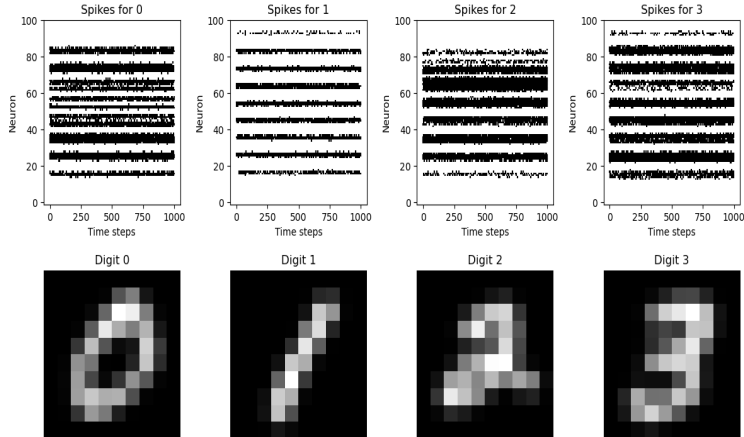


Figure 8: Figure illustrates four examples of training data from the MNIST dataset. The top row demonstrates the resulting spike-encoded training data leveraging snntorch’s `spikegen.rate()` function. The neurons are plotted against time, and each dot signifies a spike.

2.5.2 GLM-model

To quantify the effect of sleep-based regularization and provide 95% confidence intervals for the performance, we fit a hierarchical *beta regression* with

$$y_{ijkl} \sim \text{Beta}(\mu_{ijkl}, \phi), \quad (12)$$

$$\begin{aligned} \text{logit}(\mu_{ijkl}) = & \beta_0 + \beta_j^{(\text{sleep})} + \beta_k^{(\text{model})} + \beta_{jk}^{(\text{sleep} \times \text{model})} \\ & + b_l^{(\text{dataset})} + b_i^{(\text{seed})} + b_{li}^{(\text{dataset} \times \text{seed})}. \end{aligned} \quad (13)$$

where y_{ijkl} is the test accuracy with sleep rate j in model k , dataset l and seed i . Each β_j quantifies the fixed effect of using sleep rate j 's% relative to 0% sleep; all sleep-levels appear as factor variables for direct interpretability.

3 Results

The fixed-effect beta regression estimates (Table 1) statistically substantiate the observed trends. The intercept represents logit accuracy at 0% sleep for STDP-SNN model, while coefficients $\beta_{j=10} - \beta_{j=100}$ capture logit accuracy changes at each sleep level relative to this baseline. The strongest effects occur at $\beta_{j=10}$ (1.56, $p < .001$) and $\beta_{j=20}$ (1.59, $p < .001$), with progressively smaller—though still significant—effects at higher sleep levels. This pattern indicates diminishing returns beyond moderate sleep, consistent with the bias–variance tradeoff observed in other regularization schemes such as ℓ_1 and ℓ_2 regularization [Tarrès and Yao, 2013].

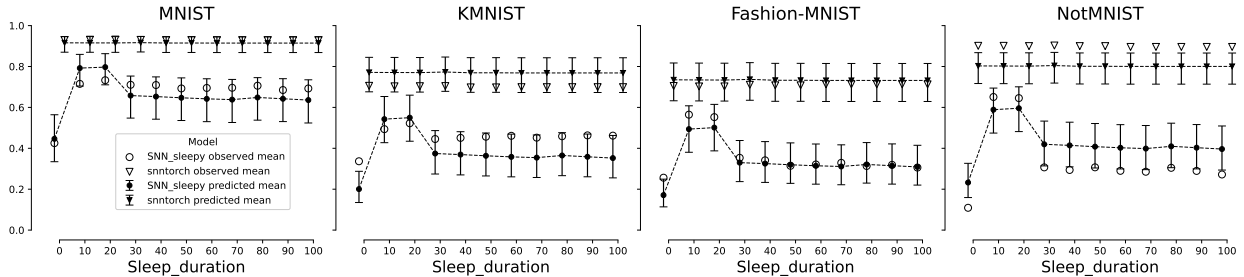


Figure 9: Mean predicted accuracy ($\pm 95\%$ CI) versus sleep duration for the STDP-SNN model and the SG-SNN model-SG across the MNIST-family benchmarks. Each point shows mean glmmTMB estimate over 5 seeds. The hollow points represent observed accuracies.

In contrast, the SG-SNN model exhibits qualitatively different behavior. The negative and significant interaction terms closely mirror the positive main effects of sleep, yielding a near-zero net effect across all sleep levels. As a result, the model performance is largely insensitive to sleep duration.

Figure 9 reflects this divergence: the SG-SNN model maintain stable, near-optimal accuracy with an optimum at 0% sleep, whereas the STDP-SNN model displays a non-monotonic response, peaking at moderate sleep (10%–20%) and declining at higher rates. This pattern is consistent across all four datasets. Despite the gains from sleep regularization, the SG-STDP model retains higher absolute accuracy overall.

Variance estimates in the lower portion of Table 1 indicate dataset-level heterogeneity, while confirming the robustness of the regularization effect.

Table 1: Mixed effect model with beta regression

Effect	Estimate	Std. Error	<i>z</i> value	<i>p</i> -value
Intercept	-1.098	.295	-3.715	.192
<i>Main effect of sleep duration</i>				
$\beta_{j=10}$	1.563	.156	10.026	< .001 ***
$\beta_{j=20}$	1.592	.156	10.212	< .001 ***
$\beta_{j=30}$.875	.152	5.764	< .001 ***
$\beta_{j=40}$.853	.152	5.619	< .001 ***
$\beta_{j=50}$.827	.152	5.444	< .001 ***
$\beta_{j=60}$.804	.152	5.295	< .001 ***
$\beta_{j=70}$.787	.152	5.190	< .001 ***
$\beta_{j=80}$.833	.152	5.497	< .001 ***
$\beta_{j=90}$.806	.152	5.298	< .001 ***
$\beta_{j=100}$.778	.152	5.118	< .001 ***
<i>Main effect of model (reference = the STDP-SNN model)</i>				
Model: SG-SNN	2.614	.167	15.657	< .001 ***
$\beta_{j=10}^{(\text{sleep} \times \text{model})}$	-1.566	.230	-6.797	< .001 ***
$\beta_{j=20}^{(\text{sleep} \times \text{model})}$	-1.599	.230	-6.939	< .001 ***
$\beta_{j=30}^{(\text{sleep} \times \text{model})}$	-.863	.228	-3.789	< .001 ***
$\beta_{j=40}^{(\text{sleep} \times \text{model})}$	-.864	.228	-3.797	< .001 ***
$\beta_{j=50}^{(\text{sleep} \times \text{model})}$	-.838	.228	-3.682	< .001 ***
$\beta_{j=60}^{(\text{sleep} \times \text{model})}$	-.819	.228	-3.600	< .001 ***
$\beta_{j=70}^{(\text{sleep} \times \text{model})}$	-.802	.228	-3.528	< .001 ***
$\beta_{j=80}^{(\text{sleep} \times \text{model})}$	-.849	.227	-3.731	< .001 ***
$\beta_{j=90}^{(\text{sleep} \times \text{model})}$	-.821	.228	-3.605	< .001 ***
$\beta_{j=100}^{(\text{sleep} \times \text{model})}$	-.793	.228	-3.483	< .001 ***
Random effect variance				
Groups	Name	Variance	Std.Dev.	
Dataset	(Intercept)	.289	.538	
Seed	(Intercept)	< .001	< .001	
Dataset:Seed	(Intercept)	.037	.192	

4 Discussion

This study shows that homeostatic, sleep-like regularization can substantially improve learning stability and generalization in locally trained SNNs—but only when applied within a narrow and well-defined regime. Across the full MNIST family of benchmarks, we find consistent

evidence that modest sleep durations yield measurable performance gains, while excessive sleep degrades learning. Together, these results present a mechanistically grounded and statistically robust account of how sleep-like processes interact with local synaptic plasticity.

The primary role of interleaved sleep phases is to prevent pathological weight growth and catastrophic interference. In recurrent SNNs trained with STDP, synaptic updates accumulate without an intrinsic normalization mechanism, leading to runaway weight magnitudes even in networks with balanced excitatory and inhibitory populations. Introducing periodic, power-law weight decay during sleep counteracts this instability by constraining synapses to remain within functional ranges. This restores effective plasticity and stabilizes learning dynamics over long training horizons.

Sleep also contributes beyond mere weight control. During sleep phases, externally driven input is removed and replaced by low-amplitude Gaussian noise, inducing spontaneous network activity. This background activity leads neurons to stochastically reactivate previously learned assemblies. Because STDP remains active during these quiescent periods, synaptic structure can be selectively reinforced without interference from new sensory patterns. This implicit replay mechanism provides a form of consolidation that may support generalization.

Crucially, our results show that the benefits of sleep are sharply bounded. For the STDP-SNN model, only mild regularization—approximately 10% – 20%—improves performance. Beyond this regime, accuracy decreases monotonically across all datasets. The beta-regression analysis in Table 1 quantifies this effect: while $\beta_{j=10}$ and $\beta_{j=20}$ are strongly positive, coefficients associated with higher sleep levels progressively diminish in magnitude and ultimately become detrimental relative to the optimal window. This pattern mirrors behavior seen in classical regularization methods (e.g., ℓ_1 or ℓ_2 penalties), where overly strong regularization increases bias and impairs performance.

Finally, our findings highlight an important interaction between learning rule and sleep efficacy. In Hebbian SNNs, sleep decay and STDP operate on compatible local activity statistics, jointly providing weight homeostasis and memory stabilization. In contrast, surrogate-gradient models exhibit a fundamentally different response. At very low sleep rates, stochastic perturbations during sleep can occasionally aid exploration of the loss landscape, yielding small performance improvements. However, as sleep duration increases, global renormalization increasingly conflicts with gradient-based optimization, potentially disrupting the coordination between error signals and weight updates. Yet, empirically, these opposing effects largely cancel out, resulting in performance that remains effectively invariant to sleep duration across the MNIST-family benchmarks.

Our implementation is amenable to neuromorphic deployment. All regularization and plasticity operations are fundamentally local, require no additional inference-time cost, and impose only $O(1)$ per-weight computational burden during sleep, thus being fully compatible with event-driven hardware.

4.1 Limitations

Several limitations should be noted. First, the number of simulation steps per sample differs between tasks (1000 ms for the geometric dataset versus 100 ms for the MNIST-family datasets). This reduction reflects computational constraints, as the MNIST-family experiments required multiple evaluations per sleep rate (five runs across eleven sleep levels),

rendering longer per-sample simulations prohibitively expensive.

Second, the SG-SNN differs fundamentally from the STDP-SNN in both learning dynamics and data representation. While the STDP-SNN relies exclusively on local spike-timing-dependent plasticity during both wake and sleep, the SG-SNN is trained via surrogate-gradient backpropagation during wake phases, with sleep introducing only stochastic weight decay and auxiliary trace-based updates. Moreover, the SG-SNN processes static pixel-valued inputs presented as continuous currents, whereas the STDP-SNN operates on spike-encoded sensory input. The two models also employ different decoding and accuracy estimation procedures. As a result, observed performance differences cannot be attributed solely to the presence or absence of sleep-based regularization, but must be interpreted in light of the distinct learning signals and representational assumptions underlying each model.

Most importantly, predictive performance of the suggested models is far from state-of-the-art, and our work should be seen as foundational for small incremental improvements of Hebbian learning within spiking neural networks, which still struggle to match the performance of regular artificial neural networks. Our work is no exception in this sense.

4.2 Future work

Several promising directions emerge from this study. First, embedding the proposed sleep regularization into deeper SNN architectures and evaluating it on larger-scale datasets would help assess scalability, robustness, and practical limitations. Extending these experiments to biologically inspired multimodal data is particularly well aligned with the biologically grounded nature of the proposed approach.

Because the sleep protocol relies on noisy membrane activity to preserve relative synaptic strengths, an important next step is to disentangle how noise contributes to this stabilization. In particular, systematically varying noise levels across different sleep rates could reveal interaction effects and clarify the conditions under which sleep most effectively supports learning.

Beyond noise-driven mechanisms, it would be valuable to examine how sleep interacts with other forms of homeostatic regulation, such as intrinsic plasticity, attentional modulation, or reward-based learning. Studying these interactions may shed light on whether sleep complements or competes with alternative stabilization strategies.

Finally, deploying the proposed models on neuromorphic hardware would provide a compelling test of their real-world applicability, while also enabling direct comparisons with other locally operating, continuous-time learning algorithms.

4.3 Conclusion

We showed that sleep-inspired homeostatic regularization can stabilize and improve locally trained STDP-based spiking neural networks, but only within a narrow operating regime. Across the MNIST-family benchmarks, moderate sleep fractions (10–20%) consistently improved performance, whereas the same intervention produced no systematic benefit in surrogate-gradient training. Using mechanistic motivation together with systematic sweeps and mixed-effects beta regression, we characterized both the benefits and limits of local sleep-based renormalization.

Although our models do not match state-of-the-art accuracy, the proposed protocol preserves strict locality and has low computational overhead, making it well suited for neuromorphic and on-chip learning. More broadly, the results suggest that sleep-like renormalization is a practical ingredient for controlling pathological weight dynamics in Hebbian SNNs, and a promising direction for biologically grounded, robust learning systems.

A Hyperparameters

Table 2: Key tuning parameters for all experiments with *the STDP-SNN model*

Component	Parameter	Descriptor	Value
Network			
	N_{in}	Input neurons	225
	N_{exc}	Excitatory neurons	200
	N_{inh}	Inhibitory neurons	50
	$P_{\text{in} \rightarrow \text{exc}}$	Wiring prob.	15%
	$P_{\text{exc} \rightarrow \text{exc}}$	Wiring prob.	10%
	$P_{\text{exc} \rightarrow \text{inh}}$	Wiring prob.	20%
	$P_{\text{inh} \rightarrow \text{exc}}$	Wiring prob.	25%
	$W_{\text{in} \rightarrow \text{exc}}$	Synaptic weight	0.10
	$W_{\text{exc} \rightarrow \text{exc}}$	Synaptic weight	0.15
	$W_{\text{inh} \rightarrow \text{exc}}$	Synaptic weight	0.30
	$W_{\text{exc} \rightarrow \text{inh}}$	Synaptic weight	-0.30
STDP			
	η_{exc}	STDP rate	5×10^{-4}
	η_{inh}	iSTDP rate	5×10^{-4}
	A_+	Potentiation	0.5
	A_-	Depression	0.3
	τ_+	LTP time constant	10 ms
	τ_-	LTD time constant	7.5 ms
Neuro-dynamics			
	Δt	Time constant	1 ms
	τ_m	Membrane time const	30 ms
	U_{rest}	Resting potential	-70 mV
	U_{reset}	Reset potential	-80 mV
	U_{max}	Max potential	40 mV
	U_{min}	Min potential	-100 mV
	R_m	Membrane resistance	30 mV
	λ_μ	Membrane noise mean	0mV
	λ_σ	Membrane noise var	3mV
	α	LIF threshold baseline	-55 mV
	τ_{th}	Threshold tc	100 ms
	δ	Thresh. jump	3
Sleep/homeostasis			
	β	Sleep percentage	10%
	α_{base}	Sleep lower bound	1.0
	λ	Sleep decay power	0.9997
	w_{tgt}	Target weight	0.2
Data processing			
	N_{train}	Training samples	6000

Component	Parameter	Descriptor	Value
	N_{test}	Test samples	1000
	N_{val}	Validation samples	100
	S_{image}	Image resize dims	(15, 15)
	f_{max}	Max spiking rate	1000 Hz
	T_{image}	Stimulus duration	100 ms
	B	Batch size	400
	N_{batches}	Number of batches	15
Early Stopping			
	p_{patience}	Training patience	0.2

Table 3: Key tuning parameters for all experiments with *the SG-SNN model*

Component	Parameter	Descriptor	Value
Network			
	N_{in}	Input neurons	225
	N_{exc}	Hidden neurons	1000
	N_{exc}	Output neurons	10
	$P_{\text{in} \rightarrow \text{hid}}$	Wiring prob.	100%
	$P_{\text{hid} \rightarrow \text{out}}$	Wiring prob.	100%
	$W_{\text{in} \rightarrow \text{hid}}$	Synaptic weight	1.0
	$W_{\text{hid} \rightarrow \text{out}}$	Synaptic weight	1.0
STDP			
	η_{exc}	STDP rate	1×10^{-3}
	η_{inh}	iSTDP rate	1×10^{-3}
	A_+	Potentiation	0.01
	A_-	Depression	0.012
	τ_{pre}	Pre-syn trace const.	20 ms
	τ_{post}	Post-syn trace const.	20 ms
Neuro-dynamics			
	Δt	Time constant	1 ms
	τ_m	Membrane decay	0.95 ms
	U_{reset}	Reset potential	0
	λ_μ	Membrane noise mean	0
	λ_σ	Membrane noise var	0.5
	α	LIF threshold baseline	1 mV
Sleep/homeostasis			
	β	Sleep percentage	[0:100%]
	α_{base}	Sleep lower bound	1.0
	λ	Sleep decay power	0.999
	w_{tgt}	Target weight	0.2
Input encoding			
	f_{max}	Max spiking rate	1000 Hz

Component	Parameter	Descriptor	Value
Data pre-processing	T_{image}	Stimulus duration	100 ms
	N_{train}	Training samples	6000
	N_{test}	Test samples	1000
	N_{val}	Validation samples	100
	S_{image}	Image resize dims	(15, 15)
	f_{max}	Max spiking rate	1000 Hz
	T_{image}	Stimulus duration	100 ms
	B	Batch size	400
Optimization	N_{batches}	Number of batches	15
	η_{Adam}	Adam learning rate	5×10^{-4}
	β_1	Adam first decay rate	0.9
	β_2	Adam sec. decay rate	0.999
Early Stopping	p_{patience}	Patience fraction	0.2
	Δ_{min}	Min. improv. thresh.	0.001

References

Alan Eric Akil, Robert Rosenbaum, and Krešimir Josić. Balanced networks under spike-time dependent plasticity. *PLOS Computational Biology*, 17(5):e1008958, May 2021. ISSN 1553-7358. doi: 10.1371/journal.pcbi.1008958. URL <https://journals.plos.org/ploscompbiol/article?id=10.1371/journal.pcbi.1008958>. Publisher: Public Library of Science.

Cristiano Capone, Elena Pastorelli, Bruno Golosio, and Pier Stanislao Paolucci. Sleep-like slow oscillations improve visual classification through synaptic homeostasis and memory association in a thalamo-cortical model. *Scientific Reports*, 9(1):8990, June 2019. ISSN 2045-2322. doi: 10.1038/s41598-019-45525-0. URL <https://www.nature.com/articles/s41598-019-45525-0>. Publisher: Nature Publishing Group.

Kristofor D. Carlson, Micah Richert, Nikil Dutt, and Jeffrey L. Krichmar. Biologically plausible models of homeostasis and STDP: Stability and learning in spiking neural networks. In *The 2013 International Joint Conference on Neural Networks (IJCNN)*, pages 1–8, August 2013. doi: 10.1109/IJCNN.2013.6706961. URL <https://ieeexplore.ieee.org/document/6706961>. ISSN: 2161-4407.

Tushar Chauhan, Timothée Masquelier, Alexandre Montlibert, and Benoit R. Cottereau. Emergence of Binocular Disparity Selectivity through Hebbian Learning. *Journal of Neuroscience*, 38(44):9563–9578, October 2018. ISSN 0270-6474, 1529-2401. doi: 10.1523/

JNEUROSCI.1259-18.2018. URL <https://www.jneurosci.org/content/38/44/9563>.
Publisher: Society for Neuroscience Section: Research Articles.

Nicolas Deperrois, Mihai A Petrovici, Walter Senn, and Jakob Jordan. Learning cortical representations through perturbed and adversarial dreaming. *eLife*, 11:e76384, April 2022. ISSN 2050-084X. doi: 10.7554/eLife.76384. URL <https://doi.org/10.7554/eLife.76384>.
Publisher: eLife Sciences Publications, Ltd.

Wei Fang, Zhaofei Yu, Yanqi Chen, Timothee Masquelier, Tiejun Huang, and Yonghong Tian. Incorporating Learnable Membrane Time Constant to Enhance Learning of Spiking Neural Networks, August 2021. URL <http://arxiv.org/abs/2007.05785>. arXiv:2007.05785 [cs].

Matthieu Gilson, Anthony Burkitt, and J. Leo van Hemmen. STDP in Recurrent Neuronal Networks. *Frontiers in Computational Neuroscience*, 4:23, September 2010. ISSN 1662-5188. doi: 10.3389/fncom.2010.00023. URL <https://pmc.ncbi.nlm.nih.gov/articles/PMC2947928/>.

Erik Hoel. The overfitted brain: Dreams evolved to assist generalization. *Patterns*, 2(5):100244, May 2021. ISSN 2666-3899. doi: 10.1016/j.patter.2021.100244. URL <https://www.sciencedirect.com/science/article/pii/S2666389921000647>.

Dongsung Huh and Terrence J. Sejnowski. Gradient Descent for Spiking Neural Networks, June 2017. URL <http://arxiv.org/abs/1706.04698>. arXiv:1706.04698 [q-bio].

Murat Isik, Karn Tiwari, Muhammed Burak Eryilmaz, and I. Can Dikmen. Accelerating Sensor Fusion in Neuromorphic Computing: A Case Study on Loihi-2, August 2024. URL <http://arxiv.org/abs/2408.16096>. arXiv:2408.16096 [cs].

Sriram Jayabal, Brandon J. Bhasin, Maxwell Kounga, Jennifer DiSanto, Aparna Suvrathan, Mark S. Goldman, and Jennifer L. Raymond. Experience Alters the Timing Rules Governing Synaptic Plasticity and Learning, December 2024. URL <https://www.biorxiv.org/content/10.1101/2022.11.28.518128v2>. Pages: 2022.11.28.518128 Section: New Results.

Fukuaki L. Kinoshita, Rikuhiro G. Yamada, Koji L. Ode, and Hiroki R. Ueda. A unified framework to model synaptic dynamics during the sleep–wake cycle. *PLOS Biology*, 23(6):e3003198, June 2025. ISSN 1545-7885. doi: 10.1371/journal.pbio.3003198. URL <https://journals.plos.org/plosbiology/article?id=10.1371/journal.pbio.3003198>. Publisher: Public Library of Science.

Yang Li, Feifei Zhao, Dongcheng Zhao, and Yi Zeng. Directly Training Temporal Spiking Neural Network with Sparse Surrogate Gradient, June 2024. URL <http://arxiv.org/abs/2406.19645>. arXiv:2406.19645 [cs].

Gehua Ma, Rui Yan, and Huajin Tang. Exploiting Noise as a Resource for Computation and Learning in Spiking Neural Networks. *Patterns*, 4(10):100831, October 2023. ISSN 26663899. doi: 10.1016/j.patter.2023.100831. URL <http://arxiv.org/abs/2305.16044>. arXiv:2305.16044 [cs].

Andreas Massey. SpikingNeuralNetwork, January 2025. URL <https://github.com/AndrlmMass/SpikingNeuralNetwork>.

Andrew Thomas Nere, Atif Hashmi, Chiara Cirelli, and Giulio Tononi. Sleep-Dependent Synaptic Down-Selection (I): Modeling the Benefits of Sleep on Memory Consolidation and Integration. *Frontiers in Neurology*, 4, September 2013. ISSN 1664-2295. doi: 10.3389/fneur.2013.00143. URL <https://www.frontiersin.org/journals/neurology/articles/10.3389/fneur.2013.00143/full>. Publisher: Frontiers.

Ning Qiao, Giacomo Indiveri, and Chiara Bartolozzi. Automatic gain control of ultra-low leakage synaptic scaling homeostatic plasticity circuits. In *2016 IEEE Biomedical Circuits and Systems Conference (BioCAS)*, pages 156–159, October 2016. doi: 10.1109/BioCAS.2016.7833755. URL <https://ieeexplore.ieee.org/document/7833755>.

Sen Song, Kenneth D. Miller, and L. F. Abbott. Competitive Hebbian learning through spike-timing-dependent synaptic plasticity. *Nature Neuroscience*, 3(9):919–926, September 2000. ISSN 1546-1726. doi: 10.1038/78829. URL https://www.nature.com/articles/nn0900_919. Publisher: Nature Publishing Group.

Peter G. Stratton, Andrew Wabnitz, Chip Essam, Allen Cheung, and Tara J. Hamilton. Making a Spiking Net Work: Robust brain-like unsupervised machine learning, September 2022. URL <http://arxiv.org/abs/2208.01204>. arXiv:2208.01204 [cs].

Qiaoyi Su, Yuhong Chou, Yifan Hu, Jianing Li, Shijie Mei, Ziyang Zhang, and Guoqi Li. Deep Directly-Trained Spiking Neural Networks for Object Detection. In *2023 IEEE/CVF International Conference on Computer Vision (ICCV)*, pages 6532–6542, October 2023. doi: 10.1109/ICCV51070.2023.00603. URL <https://ieeexplore.ieee.org/document/10376840>. ISSN: 2380-7504.

Timothy Tadros, Giri P. Krishnan, Ramyaa Ramyaa, and Maxim Bazhenov. Sleep-like unsupervised replay reduces catastrophic forgetting in artificial neural networks. *Nature Communications*, 13(1):7742, December 2022. ISSN 2041-1723. doi: 10.1038/s41467-022-34938-7. URL <https://www.nature.com/articles/s41467-022-34938-7>. Publisher: Nature Publishing Group.

Pierre Tarrès and Yuan Yao. Online Learning as Stochastic Approximation of Regularization Paths, January 2013. URL <http://arxiv.org/abs/1103.5538>. arXiv:1103.5538 [math].

Johannes Thiele, Peter Diehl, and Matthew Cook. A wake-sleep algorithm for recurrent, spiking neural networks, March 2017. URL <http://arxiv.org/abs/1703.06290>. arXiv:1703.06290 [cs].

Giulio Tononi and Chiara Cirelli. Sleep and the Price of Plasticity: From Synaptic and Cellular Homeostasis to Memory Consolidation and Integration. *Neuron*, 81(1):12–34, January 2014. ISSN 0896-6273. doi: 10.1016/j.neuron.2013.12.025. URL <https://pmc.ncbi.nlm.nih.gov/articles/PMC3921176/>.

Guan Wang, Yuhao Sun, Sijie Cheng, and Sen Song. Evolving Connectivity for Recurrent Spiking Neural Networks, May 2023. URL <http://arxiv.org/abs/2305.17650>. arXiv:2305.17650 [cs].

Friedemann Zenke, Everton J. Agnes, and Wulfram Gerstner. Diverse synaptic plasticity mechanisms orchestrated to form and retrieve memories in spiking neural networks. *Nature Communications*, 6(1):6922, April 2015. ISSN 2041-1723. doi: 10.1038/ncomms7922. URL <https://www.nature.com/articles/ncomms7922>. Publisher: Nature Publishing Group.